Emission in the ion cyclotron range of frequencies (ICE) on NSTX and NSTX-U

Cite as: Phys. Plasmas **26**, 032111 (2019); https://doi.org/10.1063/1.5081047
Submitted: 13 November 2018 . Accepted: 08 February 2019 . Published Online: 22 March 2019

E. D. Fredrickson, N. N. Gorelenkov, R. E. Bell, A. Diallo, B. P. LeBlanc, M. Podestà, and NSTX Team

Physics of Plasmas ARTICLE scitation.org/journal/php

Emission in the ion cyclotron range of frequencies (ICE) on NSTX and NSTX-U

Cite as: Phys. Plasmas **26**, 032111 (2019); doi: 10.1063/1.5081047
Submitted: 13 November 2018 · Accepted: 8 February 2019 ·
Published Online: 22 March 2019

E. D. Fredrickson,[a] N. N. Gorelenkov, R. E. Bell, A. Diallo, B. P. LeBlanc, M. Podestà, and NSTX Team

AFFILIATIONS

Princeton Plasma Physics Laboratory, Princeton, New Jersey 08543, USA

[a]eric@pppl.gov

ABSTRACT

We report here on observations of magnetic fluctuations in the ion-cyclotron frequency range on NSTX and NSTX-U. In many respects, the fluctuations appear similar to the ion cyclotron emission (ICE) seen in conventional tokamaks. However, a significant difference between previous observations of ICE and the ICE on NSTX is that the frequency of ICE in conventional tokamaks is typically near the ion cyclotron frequency of the energetic fast ions at the plasma edge. In NSTX and NSTX-U, the magnetic fluctuation frequency corresponds to the ion cyclotron frequency deeper in the plasma, near the location of an internal transport barrier. As on conventional tokamaks, higher harmonics of the deuterium cyclotron frequency, as high as the seventh, are seen with the strongest signal sometimes from higher harmonics. The emission usually appears as an irregular sequence of short bursts typically $\leq$100 μs in duration although nearly continuous emission for several ms has also been seen under some conditions. Measurements of the emission with a toroidal array of fast probes show that the emission is a long wavelength, spatially coherent mode. The emission frequency does not follow an Alfvénic scaling with density, as seen for compressional Alfvén eigenmodes, but does show a linear scaling with local magnetic field strength. The measured emission shows a compressional polarization consistent with a compressional Alfvén wave. No correlation between the neutron rate and the ICE amplitude is seen. Three-wave coupling between the instability responsible for the ICE and lower frequency modes has also been observed.

I. INTRODUCTION

Extensive measurements have been made of super-thermal wave emission in the ion-cyclotron frequency range from laboratory plasmas.[1–19] The emission is commonly referred to as ion cyclotron emission or ICE. For tokamaks, the emission typically has some universal characteristics. The ICE appears as a sequence of narrow frequency peaks at multiples of the edge ion cyclotron frequency of super-thermal ions created by neutral beam injection, radio-frequency heating of a minority ion population, or fusion reactions. Sometimes at higher harmonics, a broad continuum of emission is also seen. Where measurements have been made, the ICE tends to have long wavelengths.[11] Under some conditions, the amplitude of ICE emission is found to be proportional to the fusion neutron rate, sparking ongoing interest in the possibility of using measurements of ICE to infer the characteristics of the confined super-thermal ion population, most importantly those originating from fusion reactions.[20–25] A complete theoretical understanding of ICE is lacking, and an improved theoretical understanding is necessary if ICE is to be used as a diagnostic of confined fast ions. Measurements of ICE on spherical tokamaks, with low magnetic fields and beam energies similar to those on higher field tokamaks, provide data from a new parameter regime to test theoretical models for ICE.

Theoretical models based on Alfvén waves,[26–33] Ion Bernstein Waves (IBW),[1,2,5,20,23,34] and spin-flip MASER emission from fusion protons[33] have been proposed to explain ICE. The apparent electromagnetic character of the emission has focussed most of the attention on Alfvén wave based models such as the magneto-acoustic cyclotron instability (MCI) or Alfvén Cyclotron Instability (ACI). In these models, compressional Alfvén waves are excited through a Doppler shifted ion cyclotron resonance.[26–33] The models predict that the compressional Alfvén eigenmodes (CAEs) would be excited near the plasma edge by an anisotropic fast ion distribution of barely trapped fusion products or beam ions. The requirement of the resonance means that frequencies should be down-shifted by the parallel motion of the fast ions from the fast-ion cyclotron frequency. The down-shifted ICE frequency would help avoid potentially strong ion-cyclotron damping of the emission by the thermal plasma but would represent a relatively small shift from the ion cyclotron frequency in tokamaks like TFTR and JET.

Early beam heating experiments on spherical tokamaks saw a broad spectrum of modes,[35–40] some of which are identified as Doppler-shifted cyclotron resonance driven CAE.[38,39] The frequency down-shift is relatively large on spherical tokamaks, which have much lower toroidal fields, thus lower cyclotron frequencies, than conventional tokamaks, but similar beam ion energies. The counter-propagating CAE typically has frequencies of order half the edge deuterium ion-cyclotron frequency, consistent with the expected downshift from the co-injected neutral beams. These modes were suggested to be the manifestation of ICE in spherical tokamaks.[27,28] Co-propagating CAE with frequencies up to and exceeding the edge ion-cyclotron frequency were seen on MAST[40] and NSTX.[39] The resonant fast ion drive for co-propagating CAE with frequencies approaching, but below, the edge cyclotron frequency is generally not considered to be through a cyclotron resonance as the Doppler-shifted resonance condition would not be satisfied.

Here, we report on observations of a highly coherent instability in the deuterium ion cyclotron frequency range on NSTX[42] and NSTX-U.[43] The pulse length, maximum plasma current, and toroidal field were increased, and three neutral beam sources were added in the upgrade from NSTX to NSTX-U. NSTX/NSTX-U is a low aspect ratio tokamak with a major radius of ≈90 cm and a minor radius of ≈60 cm. ICE was measured in NSTX plasmas with nominal toroidal field strengths from 2.6 kG up to 4.6 kG. The NSTX-U shots during the commissioning campaign were taken mostly with a toroidal field of 5.9 kG. (Throughout this paper, the toroidal field numbers, unless otherwise noted, refer to the vacuum field at a major radius of 100 cm.) The plasmas were heated with up to 7 MW of neutral beams with energies of up to 100 keV. The ICE is typically seen at low density early in the discharges, often during the current ramps, and so, the plasma currents ranged from 0.35 MA up to 1.1 MA.

II. PRINCIPAL OBSERVATIONS

In this section, we will describe the physical characteristics of the ICE seen on NSTX and NSTX-U, particularly how these observations are similar to, or different from, ICE measurements on conventional aspect ratio tokamaks. The theoretical models for previous observations of ICE interpreted it as an Alfvénic instability.[26–33] Thus, we will also compare the characteristics of the spherical tokamak ICE observations with previous studies of compressional Alfvén eigenmodes (CAEs) on NSTX and MAST. We will begin with a documentation of the dependence of the ICE frequency on plasma parameters.

Examples of ICE are shown in Figs. 1 for NSTX and 2 for NSTX-U. The spectrograms in Figs. 1 and 2 are of magnetic fluctuations measured with a Mirnov coil mounted on the vacuum vessel wall and located approximately 20 cm from the plasma edge. Two experimental campaigns on NSTX had Mirnov coil data acquired at a sufficiently high rate for ICE measurements. In the 2002 campaign, a single Mirnov coil was acquired at 10 MHz (e.g., Fig. 1). The 2004 campaign had a four-coil array acquired at 10 MHz and a separate twelve-coil array acquired at 4 MHz. The 2016 NSTX-U campaign had a 15 coil array acquired at 10 MHz (and at 15 MHz for a few shots). The Mirnov coils on NSTX had a bandwidth of ≈1.8 MHz and were re-designed for NSTX-U to extend the bandwidth to ≈3 MHz. Above the nominal bandwidth (1.8 MHz or 3 MHz), the Mirnov sensor response falls off approximately inversely with frequency, and there are no anti-aliasing filters. The Mirnov coil arrays are configured to

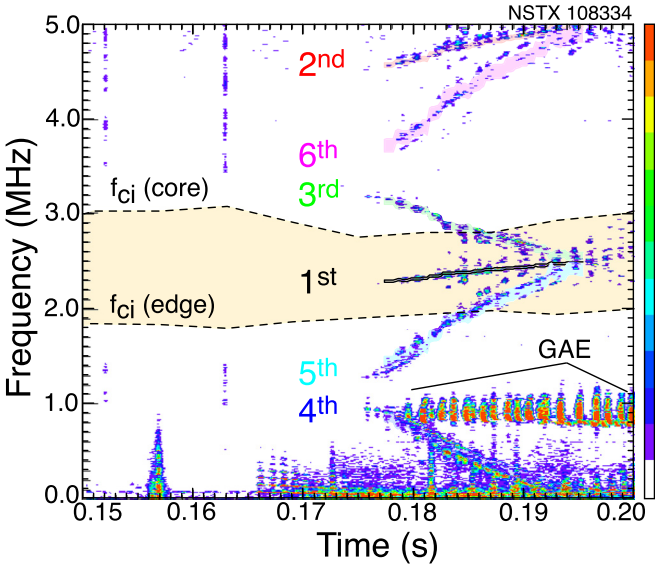

FIG. 1. Spectrogram of magnetic fluctuations with the fundamental ICE harmonic in the high-lighted area; frequencies of aliased harmonics indicated by colored bands ($\delta f/f \approx 1.5\%$). $P_{NBI} \approx 1.7$ MW; $B_{tor} \approx 3.4$ kG; acquisition rate, 10 MHz; the spectrogram is created with multiple 8092 point windowed ffts; the colorbar is linear with arbitrary units.

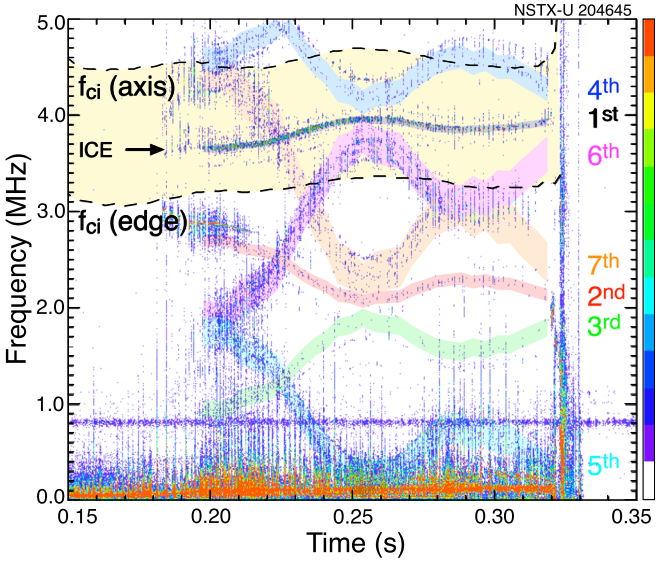

FIG. 2. Spectrogram of magnetic fluctuations acquired at a digitization rate of 10 MHz. The shaded region shows the range of f_{ci} values from the plasma edge to the axis, the colored bands ($\delta f/f \approx 1\%$) show aliased harmonics of the fundamental f_{ci} for deuterium, as indicated. $I_P \approx 0.6$ MA; $P_{NBI} \approx 5.8$ MW; $B_{tor} \approx 5.9$ kG; acquisition rate, 10 MHz; the spectrogram is created with multiple 2048 point windowed ffts; the colorbar is linear with arbitrary units; and the 800 kHz band is noise from error-field correction power supplies.

measure both poloidal and toroidal magnetic fluctuations on both NSTX and NSTX-U, the toroidal mode number of coherent modes, and provide some limited information on the poloidal structure.

A. ICE frequency higher than edge ion cyclotron frequency

The ion cyclotron emission seen on NSTX/NSTX-U is similar in many ways to the ICE commonly seen in conventional aspect ratio tokamaks, with some interesting exceptions, and is qualitatively different from the CAE seen on NSTX and MAST. The most significant difference between ICE on conventional tokamaks and ICE on NSTX/NSTX-U is that the ICE frequency is significantly higher than the edge cyclotron frequency, but lower than that on the axis. ICE frequencies on conventional tokamaks are typically found to be near harmonics of the cyclotron frequency of the energetic ion species at the outboard plasma edge. The exceptions are cases where emission maps to the magnetic axis.[14–18] In contrast, the frequency of ICE measured on NSTX and NSTX-U is approximately half way between the edge and the core ion-cyclotron frequency. This is seen in Fig. 1 for a 3.4 kG NSTX shot, and in Fig. 2 for a 5.9 kG NSTX-U shot. There is a narrow band of magnetic fluctuations, identified in Fig. 1 as ICE, whose frequency varies from ≈2.3 MHz at 0.175 s up to ≈2.5 MHz at 0.195 s. The yellow-shaded band spans the range of fundamental deuterium ion-cyclotron frequencies from the outboard plasma edge to the magnetic axis. The ICE frequency within each shot increases as the plasma is moved inward in the major radius to a higher field, demonstrating the cyclotron frequency scaling of the ICE. The ICE frequency mapping to an ion-cyclotron resonance deeper in the plasma presents a challenge to theory which predicts, among other things, that the ICE should be strongly damped by the cyclotron resonance with the thermal ions.

As with observations of ICE on higher field tokamaks, higher harmonics (up to the seventh) have been seen on NSTX/NSTX-U. This is in contrast to the CAE studied on NSTX where higher harmonics, while theoretically possible, are not seen. The diagnostic systems on NSTX and NSTX-U were not designed to study instabilities with frequencies above the ion cyclotron frequency, and the higher ICE harmonics are typically aliased, complicating interpretation of the spectra. The aliased higher harmonics are seen in Figs. 1 and 2 and are identified by mapping the expected harmonic frequencies, based on the fundamental harmonic frequency, onto the spectrogram as the labeled colored bands.

ICE has been associated with various fast ion populations, including fusion products, RF tail ions, and beam ions. The fusion alphas born on barely confined orbits were assumed to provide the drive for ICE on JET, and the ICE amplitude tracked the calculated alpha population over several orders of magnitude. The dominant energetic particle species in the NSTX/NSTX-U plasmas are the deuterium neutral beam ions. However, the D-D fusion reactions produce three other fast-ion species in roughly equal numbers, 1.01 MeV Tritons, 3.02 MeV protons, and 0.82 MeV He^3 which could, in principle, excite the ICE. We can estimate an upper limit for the fusion product populations by assuming no losses and neglecting slowing down. Then, the total number of fusion product ions can be estimated from the integral in time of the total neutron rate, S (neglecting losses, all D-D fusion products would have roughly the same density). This yields $N_{fp} = \int S/2\, dt \approx 1 \times 10^{12}$ at 0.22 s for the case of the shot shown in Fig. 2. The NUBEAM module[44] in TRANSP[45] calculates the volume integral of beam ions to be $N_{bm} \approx 4.5 \times 10^{17}$ at 0.22 s, and so, the maximum average relative density of each of the fusion products is $N_{fp}/N_{bm} \approx 2.2 \times 10^{-6}$, much smaller than the average beam-ion density. Further, the very energetic fusion products are susceptible of large losses as a result of the large radial excursions of their orbits. For example, in the 2.6 kG plasmas, the toroidal Larmor radius of the tritons and protons is ≈60 cm, and for the He^3, the Larmor radius is ≈30 cm; thus, a large fraction of the fusion products is likely to be lost. In Fig. 3 are shown the profiles of the ion cyclotron frequencies for the D-D fusion products (tritium, helium-3, and hydrogen) and deuterium *vs.* major radius and the measured ICE frequency (vertical dashed line) for the plasma shown in Fig. 2 (at 0.298 s). The ICE frequency is significantly lower than the edge cyclotron frequencies for the proton (H) and He^3. The tritium cyclotron frequency is well below the measured ICE frequency. The ICE is thus reasonably assumed to be driven by the non-thermal deuterium beam ions.

In Fig. 4(a) are shown contours of the density profile (black) for the shot shown in Fig. 2. The deuterium ion cyclotron frequency, $f_{ci}(R)$, varies from somewhat greater than 5 MHz at a major radius of 0.9 m to about 3 MHz at a major radius of 1.6 m in Fig. 4. The 3 MHz to 5 MHz part of the magnetic fluctuation spectrum can be mapped to the major radius using $f_{ci}(R)$, as long as $f_{ci}(R)$ is monotonic. In Fig. 4(a), the ICE frequency spectrum (red contours) is time-dependently mapped to the major radius using $f_{ci}(R,t)$ and overlaid on the density contours. The blue curve in Fig. 4(a) indicates the location of the magnetic axis. The evolution of the ICE frequency is correlated with the movement of the plasma, that is, as the plasma is shifted inwards towards higher magnetic field, the ICE frequency increases. The radial location of the mapped ICE frequency peak roughly follows the contours of density or perhaps, more accurately, follows the location of an apparent internal transport barrier. Here, the "transport barrier" refers to a region with a strong local radial gradient, for example, the blue-shaded region for T_i in Fig. 5(b), 1.20 m ≤ R ≤ 1.29 m. [A region of

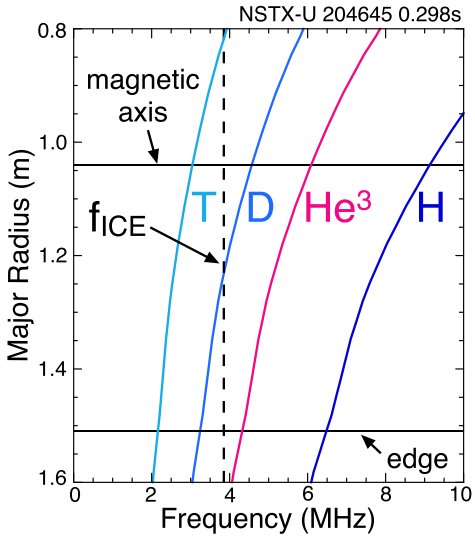

FIG. 3. Cyclotron frequency profiles for the principal energetic ion species, compared to the ICE frequency.

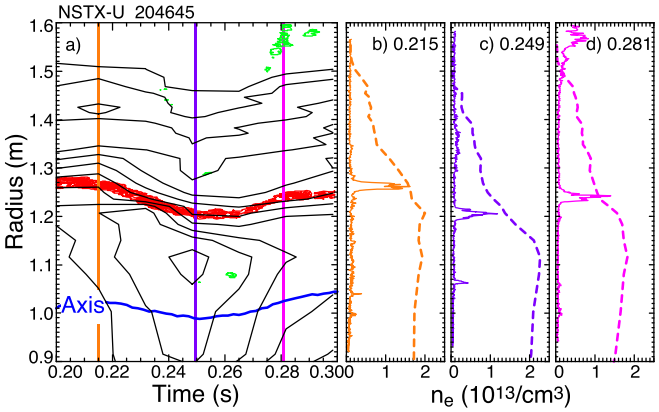

FIG. 4. (a) Contours of electron density (black) with a magnetic spectrogram overlaid (red—fundamental, green—higher harmonics), where the spectrogram frequency has been mapped to the radial profile of the ion-cyclotron frequency. The blue curve shows the location of the magnetic axis and (b)–(d) the density profile and fluctuation spectra (a.u.) mapped to the radius at indicated times.

steep gradient would be indicated by compressed contours in Figs. 4(a) or 5(a).]

The correlation with the transport barrier is seen more clearly in the time slices of the magnetic fluctuation spectrum and the density profile at 0.215 s, 0.249 s, and 0.281 s in Figs. 4(b)–4(d), respectively. The ICE maps to a region of the strong local density gradient in ≈80% of the approximately 100 shots from NSTX-U examined so far. In other words, the ICE maps just inside, or just outside, the strong density gradient region, or there was not a strong local density internal transport barrier. This location is also typically near a local minimum in the radial profile of the Alfvén velocity. Similar observations were made for the earlier NSTX shots.

The internal density transport barrier also approximately coincides with momentum and ion temperature transport barriers. We show in Fig. 5 data from a shot similar to those shown in Fig. 4. This shot also had the inward and then outward motion of the strong density gradient region as seen in Fig. 5(a). Profiles of the toroidal velocity

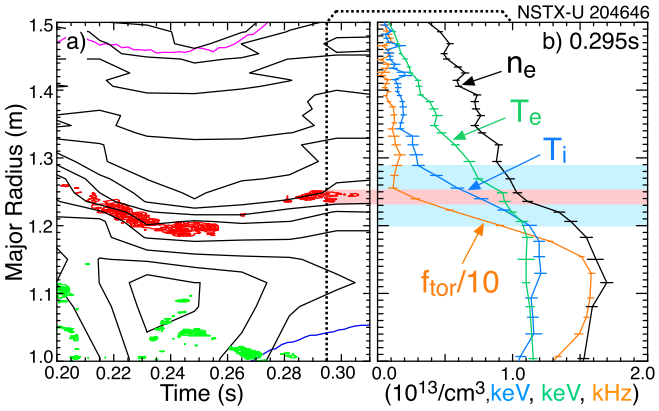

FIG. 5. (a) ICE spectrogram mapped to the major radius (red) overlaid on density contours (black), (b) magnetic fluctuation spectrum mapped to the major radius (red), electron density (black), and ion temperature (blue) profiles at 0.298 s.

(shown as rotation frequency in Fig. 5(b), orange curve) and ion temperature (Fig. 5(b), blue curve) were available around 0.3 s. The electron density (black) and electron temperature (green) profiles are also shown. In this and other examples, both the toroidal velocity and the ion temperature are very low outside the mapped radius of the ICE. This is even true in H-mode cases where the radial change in density can be quite small at the mapped ICE location, but the ion temperature still remains very low outside the ICE radius, while the ICE is present. The lower ion temperature may reduce thermal ion damping of the ICE.

In Fig. 6 is shown an example of ICE during an H-mode transition in NSTX-U. In Fig. 6(a), the spectrogram shows the ICE frequency slowly increasing in time, consistent with a small inward motion of the plasma. In Fig. 6(b), the magnetic fluctuation spectrum is mapped to the major radius using $f_{ci}(R,t)$ and overlaid on contours of density. This plasma density was increasing prior to the H-mode transition, and the density continued to increase afterwards. While the internal transport barrier present in the L-mode phase fades after the

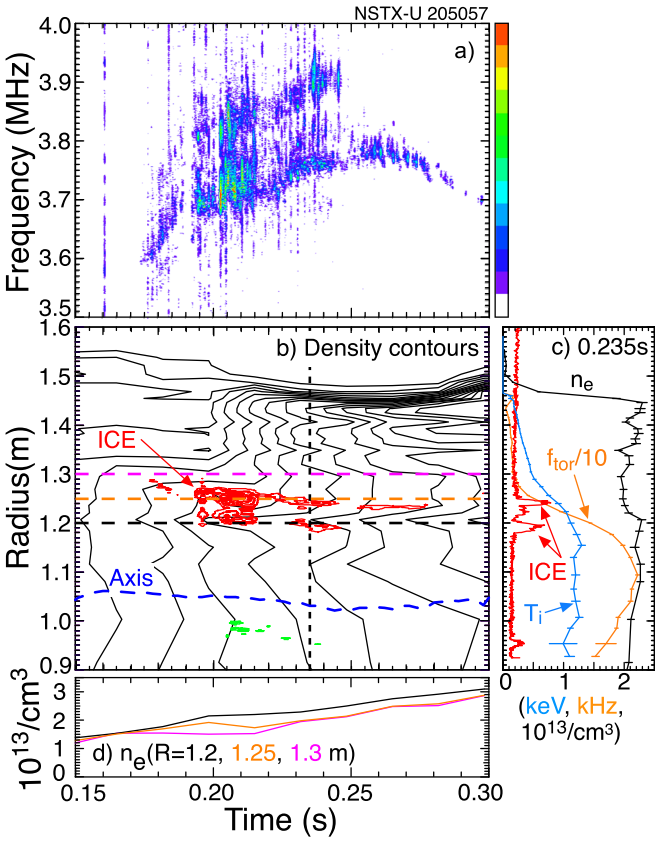

FIG. 6. (a) Magnetic fluctuation spectrum showing ICE, (b) Contours of electron density (black) with the magnetic spectrogram overlaid (red), where spectrogram frequency has been mapped to the major radius, (c) density profile (black), fluctuation spectra (red), rotation frequency (yellow), and ion temperature (blue) at ≈0.235 s [dashed line in 7(b)], and (d) density evolution at three major radii, black at R = 1.2 m, red at R = 1.25 m, and blue at 1.3 m. $B_{tor} \approx 5.9$ kG; acquisition rate, 10 MHz; the spectrogram is created with multiple 8092 point windowed ffts; and the colorbar is linear with arbitrary units.

H-mode transition, the mapped ICE location remains correlated with a residual inflection in the density gradient and with the ion temperature and velocity transport barriers as seen in Fig. 6(c). This example is primarily of interest in that the density increases substantially during the period of ICE emission. The density increase is clear in Fig. 6(d) where the density roughly doubles between 0.15 s and 0.3 s at the major radius of the mapped ICE location. The wave frequency increases slightly as the density increases, rather than dropping by roughly 40% that would be expected for an Alfvénic mode. The predicted 40% drop in frequency is supported by simulations with the CAE code.[41] This independence of the ICE frequency from plasma density was also observed in experiments on LHD[13] and TUMAN-3M.[14] In contrast, the frequencies of CAE on NSTX show a clear Alfvénic scaling with density.

B. ICE fine-structure, bursting, and time coherence

Figure 7 shows an example of ICE where the fundamental ICE emission peak exhibits a complicated fine structure reminiscent of that reported on JET.[8] The emission comes in short, irregular bursts in roughly six frequency bands with an average spacing between bands on the order of 110 kHz or $\delta\omega/\omega \approx 2.7\%$. While the multiple frequency peaks seen near the fundamental harmonic are reminiscent of the frequency splitting reported on JET, the frequency splitting was not seen on the fundamental and second harmonic although that may have been due to the lack of resolution in the frequency spectra. On NSTX, the frequency splitting fine structure has been seen on all harmonics. On conventional tokamaks, the splitting of ICE peaks was predicted to scale like $\delta\omega/\omega \approx \rho_L/R\ V_{beam}/V_{Alfvén}\ (1+p_r^2)$ for ICE,[30,31] where p_r is the pitch of resonant fast ions, arising from drift corrections to the beam velocity. The above equation predicts a splitting of $\delta\omega/\omega \approx 15\%$ to 17%, assuming that $\rho_L/R \approx 0.08$, $V_{beam}/V_{Alfvén} \approx 1.24$–$1.45$, and $p_r \approx 0.7$, approximately six times 2.7% seen in the experiment.

The ICE is not continuous, but has a bursty character, with varying burst lengths and amplitudes. Bursting was also seen in some of the early studies of ICE on higher field tokamaks[5,13,16] although many early measurements lacked the time resolution to resolve short bursts. In Fig. 8(a) is shown a spectrogram of magnetic fluctuations covering the frequency range of the fundamental deuterium ICE showing multiple, short period bursts (data again from the example shown in Fig. 2). In Fig. 8(b) is shown the root-mean-square (rms) magnetic fluctuation level over the frequency range of 3.8 MHz up to 4.0 MHz. The period and amplitude of the bursts are irregular, but in this time interval, roughly two to three bursts per millisecond are typical.

There are four short, nearly quiescent periods between 0.24 s and 0.25 s in Fig. 8(b). These are correlated with strong bursts of Toroidal Alfvén Eigenmode (TAE) activity visible in the rms fluctuation level in

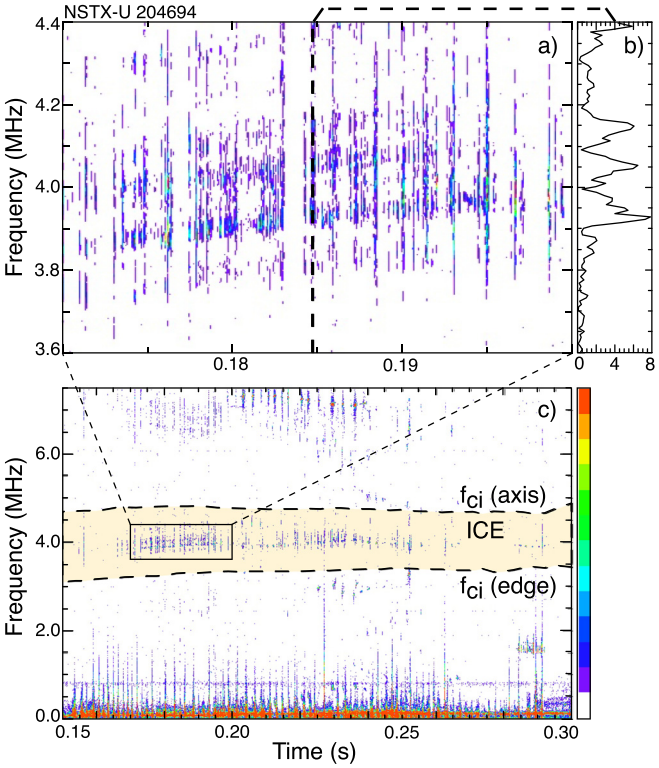

FIG. 7. (a) Detail of the spectrogram illustrating multiple frequency bands in fundamental ICE, (b) spectrum at 0.18482 s, and (c) spectrogram of magnetic fluctuations with the fundamental ICE harmonic in the high-lighted area. $I_P \approx 0.6$ MA; $P_{NBI} \approx 5.5$ MW; $B_{tor} \approx 5.9$ kG; acquisition rate, 15 MHz; the spectrogram is created with multiple 2048 point windowed ffts; and the colorbar is linear with arbitrary units.

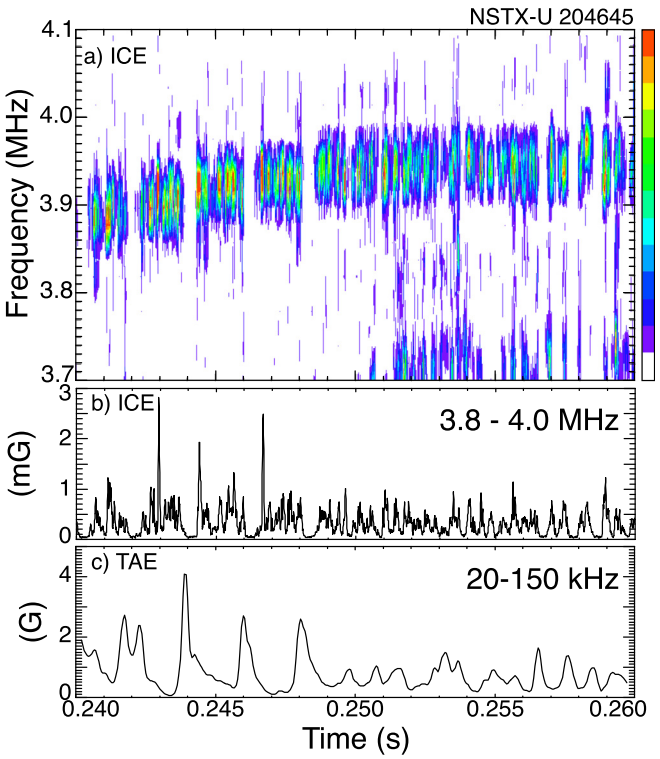

FIG. 8. (a) Spectrogram of magnetic fluctuations showing bursts of Ion Cyclotron emission, (b) rms amplitude of the ICE bursts, and (c) rms amplitude of lower frequency Toroidal Alfvén eigenmodes. The spectrogram is created with multiple, overlapping, 512 point windowed fast Fourier transforms, and the colorbar is linear with arbitrary units.

the TAE frequency range as shown in Fig. 8(c). The strong ICE bursts follow a short quiescent period after each TAE avalanche burst. The TAE avalanches are known to perturb the fast ion population by reducing the energy of the fast ions and by shifting them radially outward. Generally, ICE is believed to be excited by energetic ions near the plasma edge, and so, it is surprising that the avalanches, which move fast ions towards the plasma edge, suppressed the ICE for a short period. However, it could be consistent with an assumption that the ICE, and the fast ions that excite it, comes from deeper in the plasma, near the location of the peak TAE amplitude.

A digitally filtered Mirnov coil signal of the largest of the ICE bursts in Fig. 8(b) at ≈0.243 s is shown in Fig. 9(a). The duration of the large burst is about 100 μs. The Fourier transform of the pink region in Fig. 9(a) is shown in Fig. 9(b), where the full-width at half-maximum of the spectral peak is about 20 kHz ($\delta\omega/\omega \approx 0.5\%$), a width consistent with the duration (or growth/damping rate) of the burst, indicating that this is a very temporarily coherent signal. The peak width, normalized by the local gradient of the cyclotron frequency (≈30 kHz/cm), gives a "resonance layer" width of ≈0.7 cm, which is where the ion cyclotron frequency would match the mode frequency. The initial growth rate of this burst is $\gamma \approx 3.07 \times 10^5$/s or $\gamma/\omega \approx 1.25\%$.

Theoretical work for conventional aspect ratio tokamaks has suggested that the lower frequency harmonics are linearly stable or have lower growth rates than higher harmonics and are non-linearly excited by the higher harmonics.[21,22] This prediction is consistent with some of the experimental data on conventional aspect ratio tokamaks. On NSTX-U, the bursts at each of the harmonics are weakly correlated in time, indicating that there is indeed some coupling between harmonics, although it is not clear whether that is wave-wave coupling or a coupling through the fast ion population. The time-delay correlation of the rms-fluctuation levels, which is a correlation of the burst times, between harmonics for the data shown in Fig. 2 is shown in Fig. 10. Time-delay correlations of the rms amplitude of the fundamental harmonic with the 2nd, 4th, 6th, and 7th harmonics are shown in Figs. 10(b) through 10(e). The third harmonic was too weak, and the fifth harmonic was aliased into the lower frequency band dominated by toroidal Alfvén eigenmode activity and so could not be included. The figure covers the time range from 0.24 s to 0.275 s when these (aliased) harmonics were well separated in frequency. Time-delay correlations were calculated over the two time windows indicated by the pink and blue bands in Fig. 10(a). The harmonic bursts are correlated at the ≈50% level in each window [Figs. 10(b) through 10(e)], but the bursts

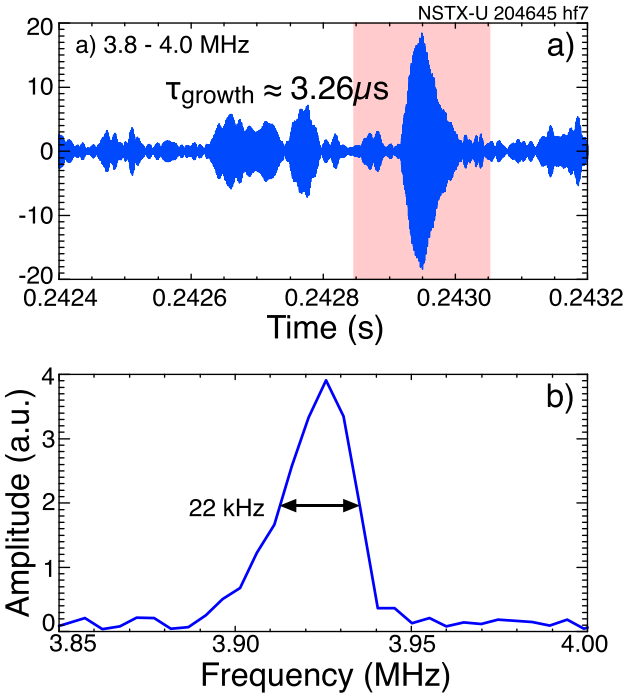

FIG. 9. (a) Digitally filtered ICE fluctuations for example shown in Fig. 4, (b) Fourier transform of the pink region in (a) showing a FWHM of ≈22 kHz. (2048 point Fourier transform and 10 MHz sample rate).

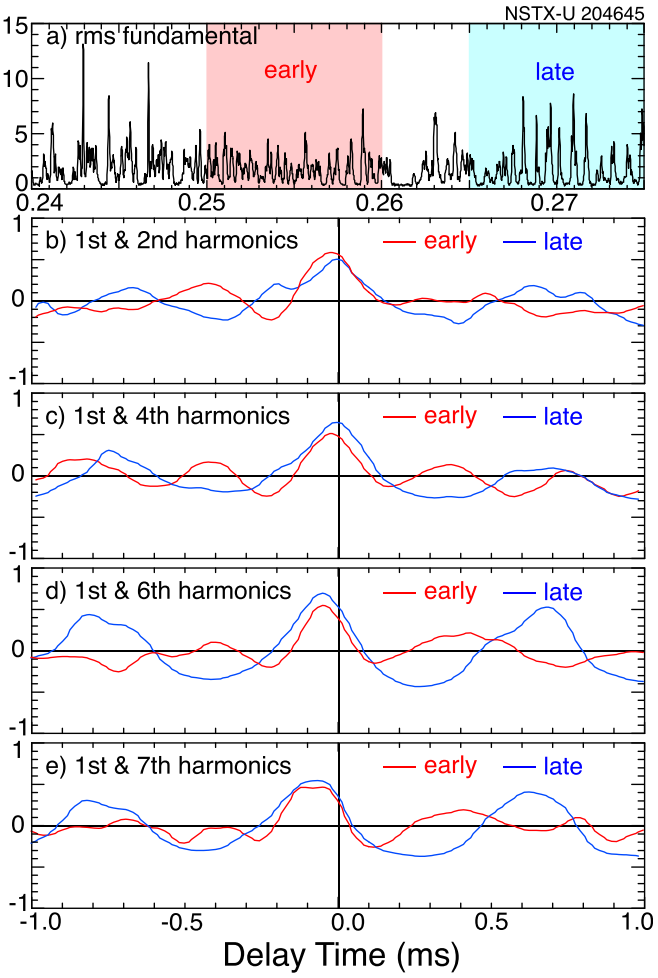

FIG. 10. Cross-correlation of fundamental ICE rms fluctuations with the 2nd, 4th, 6t,h and 7th ICE harmonics. Red curves are correlations done in the first time window indicated in 8(a) by the pink band, and blue curves are correlations done in the second time window indicated by the blue band (512 point overlapping fast Fourier transforms).

in the second window (blue) are nearly periodic, which shows up in the time-delay correlations as a roughly sinusoidal oscillation.

An interesting observation is that the bursts of higher harmonics slightly lead the bursts of the fundamental harmonic. The delay appears to increase roughly linearly with the harmonic number and is seen best in Fig. 10(e), where the 7th harmonic bursts lead the fundamental bursts by ≈80 μs. The apparent lag of the fundamental bursts is much larger than an estimate of the group delay through the sensor system (0.1 to 0.2 μs) and could indicate that bursts of higher harmonics trigger the lower harmonic bursts. Equally probable is that the bursting of the ICE represents a relaxation oscillation and that the timing of the various harmonic bursts is related to the time scale of the recovery of the fast-ion population between bursts.

In a few low field examples, the ICE was not bursting but showed as a continuous mode for bursts lasting as long as 3–4 ms. (The ICE bursts occurred between fishbone-like energetic particle modes.) This burst duration was sufficiently long so as to encompass several bursts of the lower frequency Global Alfvén eigenmodes (GAEs). This led to the interesting observation of a non-linear three-wave coupling between the GAE and the ICE. In Fig. 11 is shown a spectrogram of magnetic fluctuations covering the frequency range of 0–3 MHz. The fundamental and fourth harmonic (aliased) ICE is indicated with the numerals "1" and "4" in black and blue, respectively. Sidebands from coupling of the GAE to the fundamental ICE are clearly visible, with the ICE-GAE sidebands highlighted by the pink-shaded regions. Figure 11(b) expands a small region of the spectrogram (as indicated) showing a portion of the upper sideband of the first harmonic ICE. Figure 11(c) shows the rms amplitude of the fundamental ICE. Figure 11(d) similarly shows an expanded view of GAE activity in the same time interval, matching the spectrogram in Fig. 11(b). Similar coupling, although not as uniquely identifiable, is seen between the ICE and the lower frequency fishbone activity. The non-linear coupling of the GAE with ICE provides strong evidence that the ICE is a global eigenmode of the plasma, that is, the ICE is not localized to the plasma edge.

In the presence of a 'magnetic well', the ICE frequency peak broadens with a peak width of $\delta\omega/\omega \approx 10\%$ to 15%. This is illustrated in Figs. 12 and 13 which show the spectrum of ICE magnetic fluctuations in the wide frequency range between ≈1.5 MHz and ≈2.0 MHz. In Fig. 12, the magenta curve shows the evolution of the deuterium ion cyclotron frequency at the magnetic well minimum, which roughly follows the peak of the ICE spectrum. The blue and red curves show the ion-cyclotron frequency evolution at the magnetic axis and at the outboard midplane plasma edge, respectively, which are both higher than the ICE frequency peak. Magnetic wells are formed during high-current, high-β, and low field operation of NSTX; the relatively strong poloidal field at the plasma edge, together with the radial decay of the toroidal field on the outboard side, can create a local minimum in the mod(B) profile. As in previous examples, the frequency of the ICE can be related to the ion cyclotron frequency on the outboard side of the plasma at approximately the half-radius.

Figure 13(a) shows the radial profile of the local ion-cyclotron frequency *vs.* major radius (black curve), with a minimum near R = 1.2 m. The spectrum shown in Fig. 13(b) is time-averaged between 0.205 s and 0.215 s (the green band in Fig. 12). For previous examples, the narrow frequency peak together with the local gradient in magnetic field strength implied a strong spatial localization, $\delta R \approx 1$ cm, for the resonant drive of the ICE, despite the rather large Larmor radius (up to ≈ 15 cm) for beam ions in NSTX. Under the conditions of a magnetic well, the broadening of the ICE frequency peak and the longer magnetic field gradient scale length suggest that the ICE resonant layer could encompass a large fraction of the minor radius. The velocity profile data for this shot show a strong gradient just inside the well minimum, but no other evidence of a strong

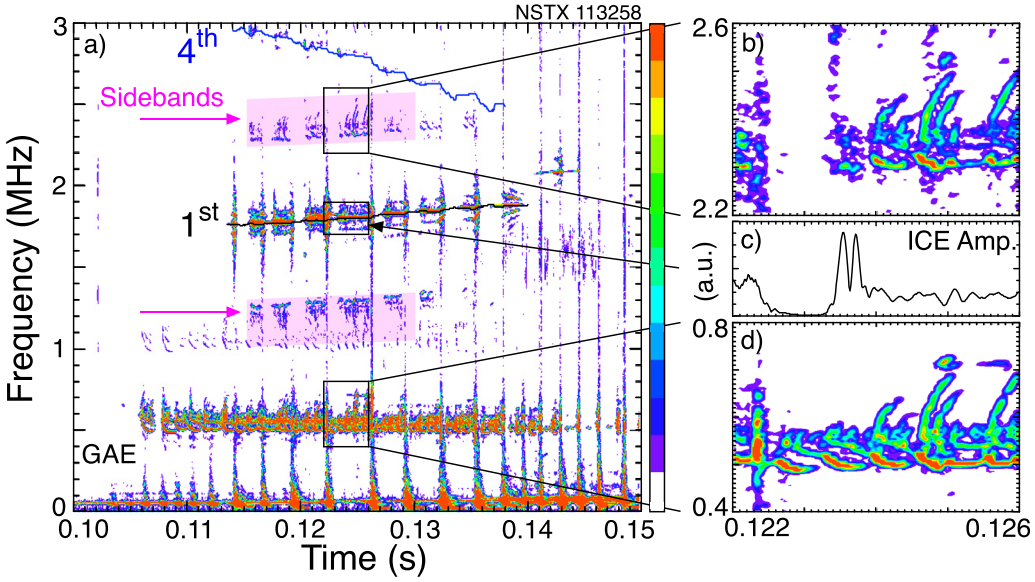

FIG. 11. (a) Spectrogram showing ICE from a 2.6 kG plasma with 3.5 MW of neutral beam heating, (b) expanded region showing the upper sideband of ICE-GAE coupling, (c) rms amplitude of fundamental ICE, and (d) expanded region showing GAE. $P_{NBI} \approx 3.5$ MW; $B_{tor} \approx 2.6$ kG; the spectrogram is created with multiple 2048 point windowed ffts; and the colorbar is linear with arbitrary units.

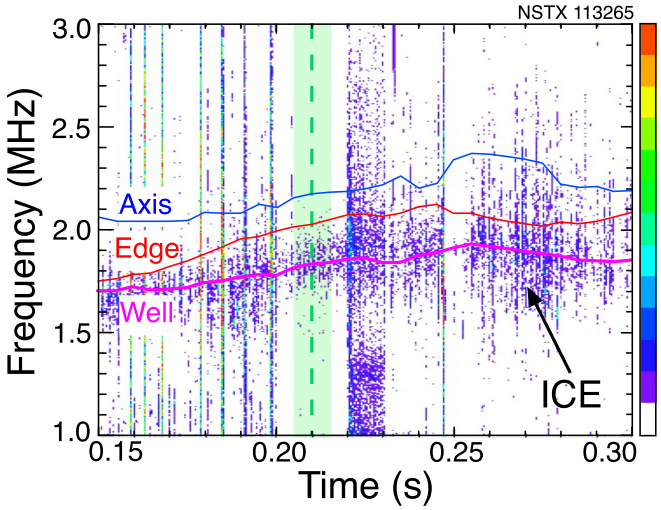

FIG. 12. (a) Spectrogram showing ICE from a 1 MA, 2.6 kG plasma with 2.7 MW of neutral beam heating. The magenta curve is the ion-cyclotron frequency at the local minimum in mod(B), and blue and red curves are the ion-cyclotron frequencies at the axis and the plasma outboard edge, respectively. $P_{NBI} \approx 4.8$ MW; $B_{tor} \approx 2.6$ kG; the spectrogram is created with multiple 2048 point windowed ffts; and the colorbar is linear with arbitrary units.

transport barrier is observed as was seen in other shots. This may represent a different type of ion-cyclotron emission.

C. Spatial structure

Measurements of the poloidal and toroidal structures of ICE have been made on the conventional aspect ratio tokamak JT-60U.[11] Toroidal propagation was found for ICE excited by fusion products, but not for the ICE associated with the deuterium beam ions. The ICE described here is measured with toroidal and poloidal arrays of magnetic sensors, offering the possibility of wavelength and mode polarization measurements.

Determination of the toroidal mode number is done by fitting the phase shifts between sensors in toroidal arrays. The configuration of the toroidal arrays and the data acquisition rates have evolved over the many experimental campaigns on NSTX/NSTX-U. Data where the Nyquist frequency of the data acquisition was greater than the fundamental ICE frequency are available from the 2002 (1 coil, 10 MHz) and 2004 (4 coils, 10 MHz, and low field shots with 12 coils, 4 MHz) NSTX campaigns and the 2016 NSTX-U campaign (15 coils, 10 MHz or 15 MHz). In intervening years, the acquisition rates were 5 MHz and 4 MHz. Configurations of the toroidal arrays for the 2002, 2004, and 2016 campaigns are shown in Fig. 14. For the 2002 campaign, only one coil was acquired at 10 MHz. Open red circles show locations of the coils in the lower bandwidth "HN" array (2004 campaign, 4 MHz). Cyan points show the locations of the four higher bandwidth coils in the NSTX "HF" array (2004 campaign, 10 MHz), and green circles show the locations of the eleven coils in the NSTX-U "HF toroidal array (2016 campaign, 10 or 15 MHz). Coils are oriented to measure vertical magnetic fluctuations, with the exception of the one NSTX HF coil and the three NSTX-U HF coils indicated with black circles, which are oriented to measure toroidal magnetic field fluctuations from which the edge magnetic fluctuation polarization can be determined.

The signal-to-noise levels for the ICE are low, and the frequencies are at or above the nominal design bandwidth of the system; so, measurements of phase-shifts between detectors are less precise than those for lower frequency, higher amplitude oscillations. The ICE also typically appear in short pulses, making discrimination against the noise background more difficult. Exceptions were found in very low

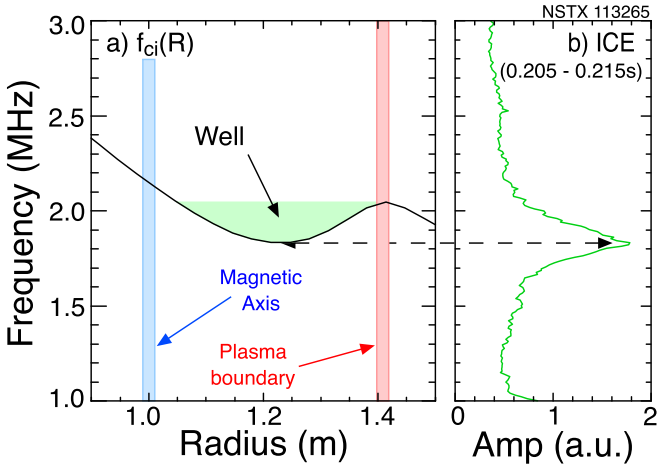

FIG. 13. (a) Profile of ion-cyclotron frequency showing the local minimum near R = 1.2 m, radii of the magnetic axis, the boundary are indicated, and (b) spectrum averaged from 0.205 to 0.215 s.

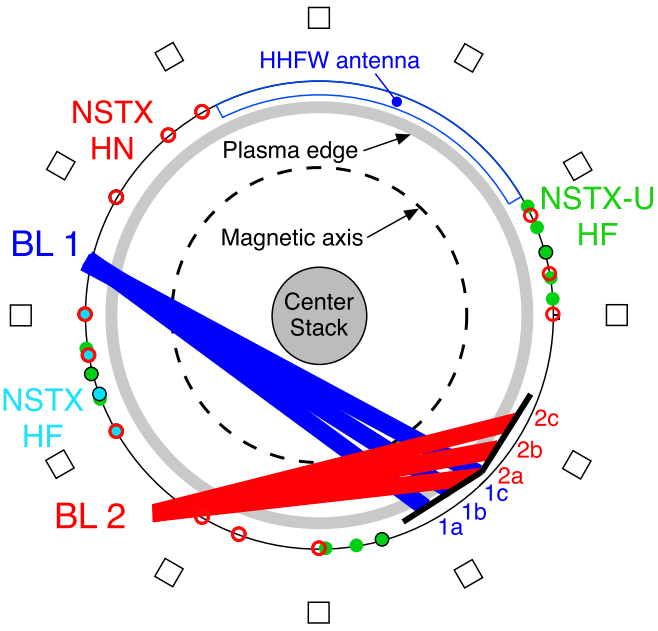

FIG. 14. Plan-view of NSTX/NSTX-U showing toroidal locations of the Mirnov arrays, beam injection trajectories, and approximate plasma magnetic axis and mid-plane boundary locations. (Find further description of this figure in the text.).

field ($B_{tor} \approx 2.6$ kG) NSTX plasmas where roughly constant ICE signals were seen lasting up to 4 ms. In some of those cases, the ICE frequency was 1.8 to 1.9 MHz which made analysis with the twelve coil array acquired at a 4 MHz digitization rate possible. The greater number of coils spanning a larger toroidal range improves the mode identification, and the results are consistent with analysis using the three-coil higher bandwidth data for that shot. The mode analysis is shown in Fig. 15 for the same shot used to illustrate 3-wave coupling of GAE with ICE in Fig. 11. The ICE is seen as the black contours between −1.8 MHz and −1.9 MHz in Fig. 15 and is counter propagating with a toroidal mode number of n = −1. The GAE is also counter propagating but with shorter wavelengths, i.e., higher toroidal mode numbers of predominantly n = −5. The spectrogram shown in Fig. 12 was made with data acquired at a rate of 10 MHz. The same mode is seen in Fig. 15 made with data acquired at 4 MHz. With the two acquisition rates of 4 MHz and 10 MHz, the mode frequency could, in principle, be ≈1.85 MHz ± 20 MHz.

In NSTX-U, the ICE frequency was near 4 MHz and mode fitting was only possible using the new toroidal array of eleven coils. The eleven coils are arranged in a toroidal array consisting of two groups of three coils and one group of five coils with the groups separated by ≈90° (Fig. 14). The distribution of the sensors into three clumps roughly 90° apart can make discrimination between n = −1 and n = +3 less certain. While the fits can be somewhat ambiguous, the best fits consistently give a counter-propagating mode with a toroidal mode number of n = −1. The mode analysis shown in Fig. 16 was done by averaging the relative phase shifts for eight separate ICE bursts. The array used on NSTX-U also includes coils oriented to measure the toroidal magnetic fluctuations. With these measurements, it was possible to determine that the magnetic fluctuations are nearly aligned with the edge equilibrium magnetic field [Fig. 16(c)], illustrating the compressional nature, as expected, for the ICE.

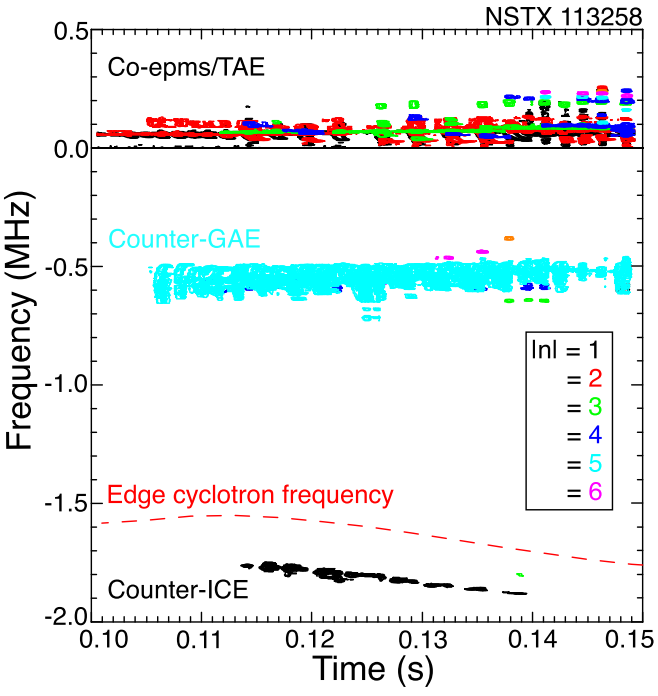

FIG. 15. Spectrogram with contours colored to indicate the toroidal mode number. Black contours at bottom are the n = −1, counter propagating ICE and cyan contours between −0.5 and −0.7 MHz are n = −5 counter propagating GAE. (Btor = 2.6 kG).

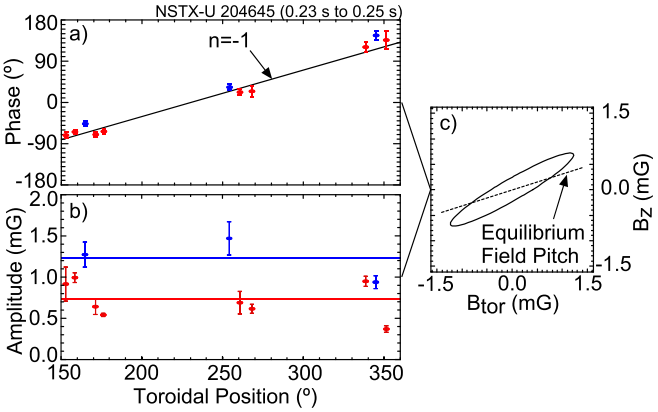

FIG. 16. (a) Phase and (b) amplitude data from the toroidal Mirnov coil array for the ICE bursts shown in Fig. 8 (red points poloidal magnetic fluctuations and blue are toroidal), (c) Composite Lissajous trace for edge magnetic fluctuations.

NSTX-U has a poloidal array of five Mirnov coils covering a vertical range of ≈0.7 m, or approximately 50°, centered on the outboard midplane. The phase and amplitude data vs. vertical displacement from the midplane (in meters) are shown in Figs. 17(a) and 17(b), respectively. For this example, there is no significant phase variation over the poloidal range of the array, indicating that there is no wave propagation in the poloidal direction. However, in other cases, poloidal propagation was seen. Determination of a poloidal mode number from a partial array such as this on the outboard side is not possible without a model for the poloidal variation of the poloidal wavelength, but the results are consistent with a small poloidal mode number.

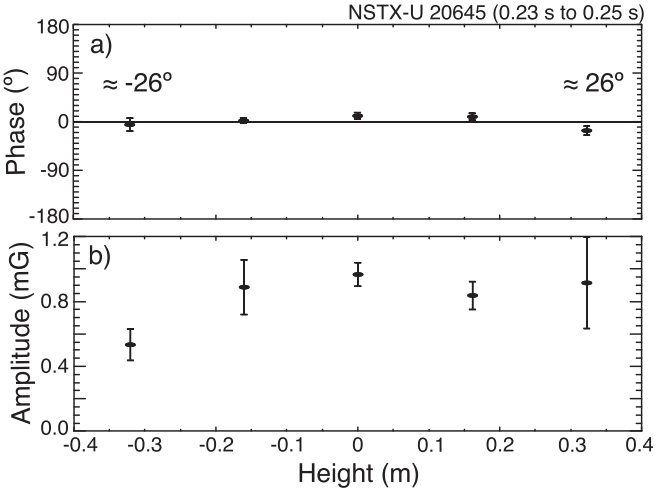

FIG. 17. (a) Phase and (b) amplitude data from the poloidal Mirnov coil array for the same ICE bursts analysed in Fig. 16.

D. Correlation of ICE with plasma parameters

A database of parameters during times of ion cyclotron emission was constructed for the NSTX-U shots in the range of 204 500–205 088. This comprises the range where noise compensation was available to reduce the broad-band pick-up from the unshielded switching power amplifiers used for error field correction. Time intervals where ICE was present were determined for each shot, and within those time intervals, plasma parameters, including parameters for each of the neutral beam sources and plasma density, were collected at the Thomson scattering times (typically, the Thomson system collects electron temperature and density profiles at a rate of 60 Hz). Spectra of magnetic fluctuations were calculated around the Thomson times and averaged over an approximately 16.7 ms window (the spacing of the Thomson scattering times). The rms fluctuation amplitude was collected in six frequency bands, with the sixth band covering the fundamental ICE frequency range of 3.5 MHz up to 4.5 MHz.

In Fig. 18 are shown the ICE frequencies normalized to the edge deuterium cyclotron frequency for early NSTX shots when a 10 MHz digitizer was available and for the NSTX-U shots. The data are graphed *vs.* the magnetic field on the axis as determined from equilibrium reconstructions, thus including paramagnetic and diamagnetic corrections as well as variations from shifts in the plasma major radius. The ICE frequencies scale roughly linearly with the toroidal field, thus maintaining a roughly constant ratio to the edge cyclotron frequency. Also shown are the frequencies from a representative sample of co-propagating CAE on NSTX, normalized to the edge deuterium cyclotron frequency. (Counter-propagating CAEs have lower frequencies, typically less than 0.4 f_{ci}.) The frequency of the co-propagating, high-n CAE in NSTX H-mode plasmas seldom exceeds the edge deuterium cyclotron frequency; however, in low density exceptions, at all toroidal fields, the co-propagating CAE can have frequencies higher than the edge deuterium cyclotron frequency. Similar observations were reported for co-propagating CAE in low field MAST plasmas.[40]

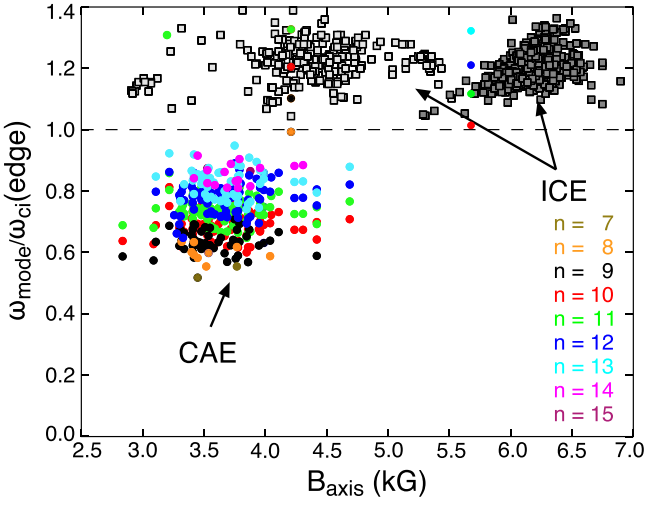

FIG. 18. Frequency of co-propagating CAE, normalized to ω_{Dci} at plasma edge vs. magnetic field on the axis. CAE toroidal mode numbers from n = 7 to n = 14 as indicated. Square points show similarly normalized ICE for NSTX (light grey) and NSTX-U (dark grey).

The frequencies of the single example, so far, of CAEs in an NSTX-U shot were all above the edge ion cyclotron frequency. As for the ICE, the normalized co-propagating-CAE frequencies appear relatively constant as the toroidal field is increased, albeit with significant scatter.

Experiments on JET found a linear correlation of the fusion products' ICE amplitude with the neutron rate.[8] The correlation of ICE intensity with the neutron rate was not so strong in TFTR, and one hypothesis for the difference was that in the JET H-mode plasmas, the fusion α's remained super-Alfvénic out to the plasma edge (but presumably not past the density pedestal). In contrast, in the higher field, peaked density TFTR supershots the fusion α's that would be sub-Alfvénic at the plasma edge.[9,29] ICE on NSTX and NSTX-U was most typically seen early in the discharge, often during the current ramp, and no clear scaling with the neutron rate was seen. The ICE was seen in relatively low density plasmas with core averaged density typically less than about $2 \times 10^{13}/\text{cm}^3$ (Fig. 19). Even at these low densities, $V_{beam}/V_{Alfvén} > 1$ at the mapped ICE location for full-energy beam ions.

E. Resonance condition and drive

In conventional tokamaks, the ICE was believed to be excited by barely confined energetic ions which create a co-propagating bump-on-tail at the plasma edge. The ICE on NSTX/NSTX-U appears to originate deeper in the plasma. However, the ICE is also most often present early in low density plasmas before the fast ion distribution has evolved to a slowing-down distribution. In Fig. 20 are shown the fast-ion distributions at five radii vs. ion energy for pitches at which bump-on-tails are observed (ICE maps to r/a ≈ 0.35). While a strong bump-on-tail is clearly visible at the plasma edge [Fig. 20(e)], inverted fast ion distributions are present at all radii, particularly at r/a ≈ 0.35, which is the approximated location where the ICE is assumed to originate. (In this plasma, three beam sources were injected with full energies of 70 keV, 80 keV, and 90 keV; the pitch at each radius was chosen to emphasize the full-energy bump-on-tail.)

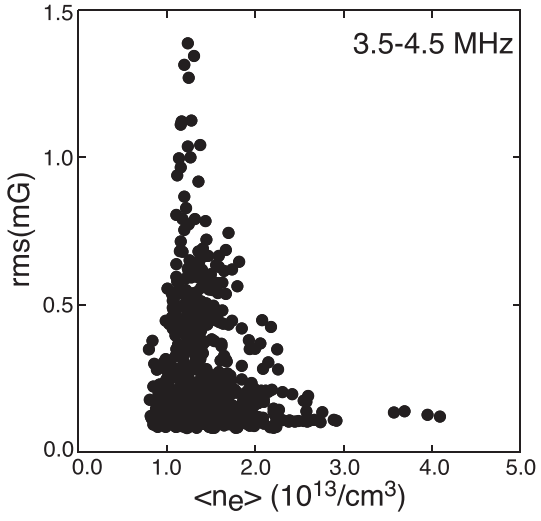

FIG. 19. Correlation of ICE intensity (fluctuation amplitude between 3.5 MHz and 4.5 MHz) and density.

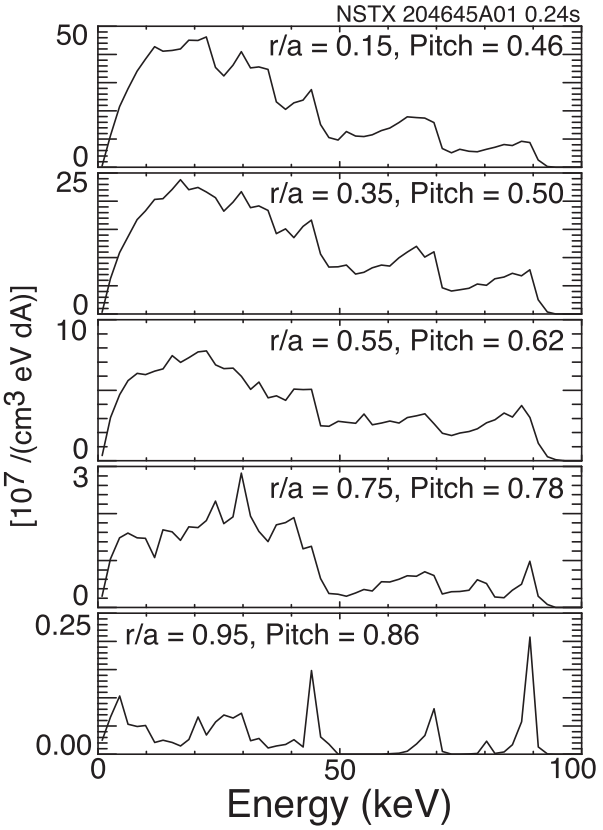

FIG. 20. Beam ion distribution function at R ≈ 120 cm showing bump-on-tails at the beam injection energies of 70 kV and 90 kV.

The resonance condition for fast ions with a co-propagating mode, including the next order fast ion drifts, is $\omega_{ICE} = \omega_{ci} + |k_{||} \pm s/qR\ |V_{b||}$. The second term on the left hand side is the Doppler-shift correction. For $n = -1$, the Doppler correction is proportional to $k_{||} \pm s/qR$, which can be written approximately as $(m\text{-}nq \pm s)/qR$, where s is an integer. Thus, for $n = -1$ and small m, this term could be nearly zero, making a plausible argument that the resonance frequency could be have a small Doppler correction from the ion cyclotron frequency. In conventional tokamaks, the Doppler down-shift of the frequency helped to alleviate damping of the ICE by the thermal plasma. In this case, where ion temperature and the density are found to be very low outside the assumed point of origin of the ICE, this thermal damping might be small enough to allow for the excitation of ICE.

III. DISCUSSION AND SUMMARY

We have described observations of highly coherent magnetic fluctuations in the ion-cyclotron frequency range on NSTX and NSTX-U which we characterize as a form of Ion Cyclotron Emission (ICE). The ICE on NSTX/NSTX-U has many similarities to the reports of ICE observations from conventional tokamaks. The ICE frequency matches the cyclotron frequency of the neutral beam ions, and multiple harmonics (up to the seventh) have been observed. As on conventional tokamaks, the emission frequency does not follow an Alfvénic scaling with density, as seen for compressional Alfvén eigenmodes, but does show a linear scaling with local magnetic field strength. Similar to previous measurements on conventional tokamaks, the emission is spatially coherent with a relatively long wavelength. As on conventional tokamaks, the frequency peaks at each harmonic can be split; however, on NSTX, the peaks may be split into two or more peaks. The ICE on NSTX/NSTX-U consists of short bursts typically 10s of μs in duration; ICE emission was also reported to have a bursting character on conventional tokamaks. No correlation between the neutron rate and the ICE amplitude is seen, consistent with some previous studies. In these respects, the ICE seen on NSTX/NSTX-U bears a strong resemblance to previous reports of ICE on conventional, higher field, tokamaks.

There are also significant differences between previous observations of ICE and the ICE on NSTX/NSTX-U. The frequency of ICE in conventional tokamaks is typically near the ion cyclotron frequency of the energetic fast ions at the plasma edge (with some exceptions). In NSTX and NSTX-U, the ICE frequency corresponds to the beam-ion cyclotron frequency deeper in the plasma, near the location of an internal velocity, or ion energy and density transport barrier. This correlation appears to be quite strong and suggests that the presence of the transport barrier plays an important role in the instability.

The low field, and hence low frequency of the ICE on NSTX and NSTX-U, allowed for new measurements of ICE characteristics, with diagnostics designed primarily for studies of lower frequency instabilities. In a few very low field cases, there was a clear identification of the ICE as an $n = -1$, counter-propagating wave. This identification of the toroidal wavelength was consistent with mode number measurements of ICE seen at higher fields although the measurements made in high field plasmas were less conclusive (due to the smaller array sizes of Mirnov coils designed for high-frequency measurements). The measured emission shows a compressional polarization consistent with the expectation that ICE is a compressional Alfvén wave or eigenmode. The clear counter-to-beam injection direction of the ICE propagation suggests that the Doppler-shifted ion-cyclotron drive model for ICE would down-shift the measured ICE frequency from the ion-cyclotron frequency by up to ≈0.47 MHz; thus, the drive for the ICE seen on NSTX/NSTX-U would originate even deeper in the plasma. However, the low, $n = -1$, toroidal mode number also means that the Doppler shift could be very small, meaning the spatial mapping of the ICE is near the internal transport barrier.

The correlation of ICE burst times between the harmonics has shown that that bursts at each of the harmonics are correlated. Further, the higher harmonic bursts lead the bursts at lower harmonics, which is consistent with the theoretical prediction for large aspect ratio tokamaks (although it is not clear that that prediction would apply to NSTX-U parameters). However, it is also seen that higher harmonics are often sufficiently weak to be below the detection threshold, suggesting that at most they might trigger marginally unstable bursts at lower harmonics, but that they do not actually drive the lower harmonic ICE.

The splitting, particularly of higher harmonics of the ICE, into two peaks was predicted theoretically. While all harmonics of the ICE on NSTX/NSTX-U, including the fundamental, are typically split, the peaks are often split into more than two peaks. Further, the width of the split is significantly smaller than the simple theoretical expression predicts.

A possibly different type of ICE was seen in low field, high beta plasmas with a magnetic well. The ICE frequency becomes much less coherent in the presence of an outboard magnetic well, and the frequency of the ICE is significantly *lower* than the edge deuterium ion-cyclotron frequency. The magnetic well was created in very low field, high current plasmas with a plasma beta of >20%. The peak of the ion cyclotron emission corresponds roughly to the deuterium ion cyclotron frequency at the well minimum. The width of the emission peak is $\delta\omega/\omega \approx 13\%$, which is much broader than the typical ICE frequency peak. The broad, quasi-coherent frequency peak and the emission frequency less than the edge frequency suggest that this type of ICE is different from the other examples shown here.

In JET, the barely confined alphas would create a co-propagating bump-on-tail at the plasma edge in the fusion-α distribution. The beam-ions in NSTX-U can produce a similar edge fast ion distribution. Beam ions deposited on the high field side of the magnetic axis can be born on orbits that take them through the plasma edge on the outboard mid-plane. This is only true for the three sources with tangency radii inboard of the magnetic axis. In Fig. 10 is shown the fast ion distribution as calculated with the NUBEAM code in TRANSP for the shot in Fig. 2. In this shot, there are two clear bump-on-tails from the beam sources 1(c) and 1(b) with tangency radii of 60 cm and 70 cm, respectively. The source voltages were 90 kV and 69 kV. There was an additional source on the outboard plasma edge, 2(b), with a tangency radius of 120 cm (outside the magnetic axis) at 80 kV, and a very weak bump-on-tail can be seen from that. The width in energy of the peaks at 69 kV and 90 kV is about $\delta E/E \approx 0.05$, which might be sufficiently narrow to satisfy the requirement for destabilizing the MCI.[25,27]

High beta, low field spherical tokamaks have opened a new regime for studies of ion cyclotron emission (ICE) from plasmas. While overall the observations of ICE on NSTX/NSTX-U bear a strong resemblance to previous studies of ICE on conventional tokamaks, the observations reported here may help guide the development of a more comprehensive model of ICE. A better understanding of ICE is necessary if ICE is to be used as a fast ion diagnostic on ITER. The data presented here are not the result of dedicated experiments, but just accumulated during a broad range of experiments to study other issues. In the future, we hope that dedicated experiments and diagnostic improvements will provide further clarification of ICE characteristics.

ACKNOWLEDGMENTS

The authors appreciate the support of the NSTX project in the construction and installation of the high-frequency magnetic sensor arrays that made these observations possible. This work was supported by U.S. DOE Contract No. DE-AC02-09CH11466.

REFERENCES

[1]J. L. Dunlap, G. R. Haste, C. E. Nielsen, H. Postma, and L. H. Reber, "Microinstability limitations of the DCX-1 energetic plasma," Phys. Fluids **9**, 199 (1966).
[2]J. L. Dunlap, C. F. Barnett, R. A. Dandi, and H. Postma, "Radiation and ion energy distributions of the DCX-1 plasma," Nucl. Fusion Suppl., Part 1 233 (1962).
[3]T. Yamamoto and T. Suito, "Excitation of ion cyclotron harmonic waves in a plasma by a perpendicularly injected electron beam," J. Phys. Soc. Jpn. **24**, 933 (1968).
[4]G. J. Greene, P. L. Colestock, E. D. Fredrickson, J. C. Hosea, K. M. McGuire, J. R. Wilson, and K. M. Young, "High frequency emission from TFTR plasmas," in *Proceedings of the 15th European Conference on Controlled Fusion and Plasma Heating*, Dubrovnik, Vol. 12B, Part I (European Physical Society, Geneva, 1988), p. 107.
[5]G. A. Cottrell and R. O. Dendy, "Superthermal radiation from fusion products in JET," Phys. Rev. Lett. **60**, 33 (1988).
[6]P. Schild, G. A. Cottrell, and R. O. Dendy, "Sawtooth oscillations in ion cyclotron emission from JET," Nucl. Fusion **29**, 834 (1989).
[7]G. J. Greene and TFTR Team, "Measurement of ion cyclotron emission and ICRF-driven waves in TFTR," in *Proceedings of the 17th European Conference on Controlled Fusion and Plasma Heating*, Amsterdam, The Netherlands, edited by G. Briffod, A. Nijsen-Vis, and F. C. Schüller (European Physical Society, Petit-Lancy, Switzerland, 1990), Part IV, Vol. 14B, p. 1540.
[8]G. A. Cottrell, V. P. Bhatnagar, O. Da Costa, R. O. Dendy, J. Jacquinot, K. G. McClements, D. C. McCune, M. F. F. Nave, P. Smeulders, and D. F. H. Start, "Ion cyclotron emission measurements during JET deuterium-tritium experiments," Nucl. Fusion **33**, 1365 (1993).
[9]S. Cauffman and R. Majeski, "Ion cyclotron emission on the Tokamak fusion test reactor," Rev. Sci. Instrum. **66**, 817 (1995).
[10]S. Cauffman, R. Majeski, K. G. McClements, and R. O. Dendy, "Alfvénic behaviour of alpha particle driven ion cyclotron emission in TFTR," Nucl. Fusion **35**, 1597 (1995).
[11]M. Ichimura, H. Higaki, S. Kakimoto, Y. Yamaguchi, K. Nemoto, M. Katano, M. Ishikawa, S. Moriyama, and T. Suzuki, "Observation of spontaneously excited waves in the ion cyclotron frequency range on JT-60U," Nucl. Fusion **48**, 035012 (2008).
[12]S. Sato, M. Ichimura, Y. Yamaguchi, M. Katano, Y. Imai, T. Murakami, Y. Miyake, T. Yokoyama, S. Moriyama, T. Kobayashi, A. Kohima, K. Shinohara, Y. Sakamoto, T. Watanabi, H Hojo, and T. Imai, "Observation of ion cyclotron emission owing to DD fusion product H ions in JT-60U," Plasma Fusion Res. **5**, S2067 (2010).
[13]K. Saito, R. Kumazawa, T. Seki, H. Kasahara, G. Nomura, F. Shimpo, H. Igami, M. Isobe, K. Ogawa, K. Toi, M. Osakabi, M. Nishiura, T. Watanabi, S. Yamamoto, M. Ichimura, and T. Mutoh, "Measurement of ion cyclotron emissions by using high-frequency magnetic probes in the LHD," Plasma Sci. Technol. **15**, 209 (2013).
[14]L. G. Askinazi, A. A. Belokurov, D. B. Gin, V. A. kornev, S. V. Lebedev, A. E. Shevelev, A. S. Tukachinsky, and N. A. Zhubr, "Ion cyclotron emission in NBI-heated plasmas in the TUMAN-3M tokamak," Nucl. Fusion **58**, 082003 (2018).
[15]H. Kimura, Y. Kusama, M. Saigusa, G. J. Kramer, K. Tobita, M. Nemoto, T. Konkoh, T. Nishitani, O. Da Costa, T. Ozeki, T. Oikawa, S. Moriyama, A. Morioka, G. Y. Fu, C. Z. Cheng, and V. I. Afanastev, "Alfvén eigenmode and energetic particle research in JT-60U," Nucl. Fusion **38**, 1303 (1998).
[16]R. D'Inca, "Ion cyclotron emission on ASDEX upgrade," Ph.D. thesis (Max Planck Institute for Plasma Physics, 2014).
[17]K. E. Thome, D. C. Pace, R. I. Pinsker, O. Meneghini, C. A. del Castillo, and Y. Zhu, Rev. Sci. Instrum. **89**, 10I102 (2018).
[18]K. E. Thome, A. Lvovskiy, S. Tang, N. A. Crocker, X. D. Du, W. W. Heidbrink, Y. B. Zhu, D. A. Spong, D. C. Pace, C. A. Paz-Soldan, R. I. Pinsker, C. S. Collins, M. A. Van Zeeland, M. E. Austin, and C. A. del Castillo, "Ion cyclotron emission on ASDEX upgrade," in *Proceedings of the 27th IAEA Fusion Energy Conference*, 22–27 October (IAEA, Vienna, Gandhinagar, India, 2018), Paper No. EX/P6-29.
[19]R. O. Dendy and K. G. McClements, "Ion cyclotron emission from fusion-born ions in large tokamak plasmas: A brief review from JET and TFTR to ITER," Plasma Phys. Controlled Fusion **57**, 044002 (2015).
[20]L. Carbajal, R. O. Dendy, S. C. Chapman, and J. W. S. Cook, "Quantifying fusion born ion populations in magnetically confined plasmas using ion cyclotron emission," Phys. Rev. Lett. **118**, 105001 (2017).
[21]K. G. McClements, R. D'Inca, R. O. Dendy, L. Carbaja, S. C. Chapman, J. W. S. Cook, R. W. Harvey, W. W. Heidbrink, and S. D. Pinches, "Fast particle-driven ion cyclotron emission (ICE) in tokamak plasmas and the case for an ICE diagnostic in ITER," Nucl. Fusion **55**, 043013 (2015).
[22]N. N. Gorelenkov, "Ion cyclotron emission studies: Retrospects and prospects," Plasma Phys. Rep. **42**, 430 (2016).

[23]N. N. Gorelenkov, "Energetic particle-driven compressional Alfvén eigenmodes and prospects for ion cyclotron emission studies in fusion plasmas," New J. Phys. **18**, 105010 (2016).
[24]R. O. Dendy, C. N. Lashmore-Davies, and K. F. Kam, Phys. Fluids B **4**, 3996 (1992).
[25]R. O. Dendy, C. N. Lashmore-Davies, and K. F. Kam, "The magnetoacoustic cyclotron instability of an extended shell distribution of energetic ions," Phys. Fluids B **5**, 1937 (1993).
[26]R. O. Dendy, C. N. Lashmore-Davies, K. G. McClements, and G. A. Cottrell, "The excitation of obliquely propagating fast Alfvén waves at fusion ion cyclotron harmonics," Phys. Plasmas **1**, 1918 (1994).
[27]N. N. Gorelenkov and C. Z. Cheng, "Alfvén cyclotron instability and ion cyclotron emission," Nucl. Fusion **35**, 1743 (1995).
[28]N. N. Gorelenkov and C. Z. Cheng, "Excitation of Alfvén cyclotron instability by charged fusion products in tokamaks," Phys. Plasmas **2**, 1961 (1995).
[29]K. G. McClements, R. O. Dendy, C. N. Lashmore-Davier, and G. A. Cottrell, "Interpretation of ion cyclotron emission from sub-Alfvénic fusion products in the tokamak fusion test reactor," Phys. Plasmas **3**, 543 (1996).
[30]T. Fülöp, Ya. I. Kolesnichenko, M. Lisak, and D. Anderson, "Origin of superthermal ion cyclotron emission in tokamaks," Nucl. Fusion **37**, 1281 (1997).
[31]T. Fülöp and M. Lisak, "Ion cyclotron emission from fusion products and beam ions in the tokamak fusion test reactor," Nucl. Fusion **38**, 761 (1998).
[32]R. O. Dendy, K. G. McClements, C. N. Lashmore-Davies, R. Majeski, and S. Cauffman, "A mechanism for beam-driven excitation of ion cyclotron harmonic waves in the tokamak fusion test reactor," Phys. Plasmas **1**, 3407 (1994).
[33]V. Arunasalam, G. J. Greene, and K. M. Young, "Ion cyclotron and spin-flip emissions from fusion products in tokamaks," Nucl. Fusion **34**, 927 (1994).
[34]K. G. McClements, M. P. Gryaznevich, S. E. Sharapov, R. J. Akers, L. C. Appel, G. F. Counsel, C. M. Roach, and R. Majeski, Plasma Phys. Controlled Fusion **41**, 661 (1999).
[35]E. D. Fredrickson, R. Bell, D. Darrow, G. Fu, N. Gorelenkov, B. LeBlanc, S. Medley, J. Menard, H. Park, L. Roquemore, S. A. Sabbagh, D. Stutman, K. Tritz, N. Crocker, S. Kubota, W. Peebles, K. C. Lee, and F. Levinton, "Collective fast ion instability-induced losses in NSTX," Phys. Plasmas **13**, 056109 (2006).
[36]L. C. Appel, T. Fülöp, M. J. Hole, H. M. Smith, S. D. Pinches, and R. G. L. Vann, Plasma Phys. Controlled Fusion **50**, 115011 (2008).
[37]M. P. Gryaznevich, S. E. Sharapov, M. Lilley, S. D. Pinches, A. R. Field, D. Howell, D. Keeling, R. Martin, H. Meyer, H. Smith, R. Vann, P. Denner, E. Verwichte, and MAST Team, "Recent experiments on Alfvén eigenmodes in MAST," Nucl. Fusion **48**, 084003 (2008).
[38]E. D. Fredrickson, N. N. Gorelenkov, M. Podesta, A. Bortolon, N. A. Crocker, S. P. Gerhardt, R. E. Bell, A. Diallo, B. LeBlanc, F. M. Levinton, and H. Yuh, "Non-linear modulation of short wavelength compressional Alfvén eigenmodes," Phys. Plasmas **20**, 042112 (2013).
[39]N. A. Crocker, E. D. Fredrickson, N. N. Gorelenkov, W. A. Peebles, S. Kubota, R. E. Bell, A. Diallo, B. P. LeBlanc, J. E. Menard, M. Podestà, K. Tritz, and H. Yuh, "Internal amplitude, structure and identification of compressional and global Alfvén eigenmodes in NSTX," Nucl. Fusion **53**, 043017 (2013).
[40]S. E. Sharapov, M. K. Lilley, R. Akers, N. Ben Ayed, M. Cecconello, J. W. S. Cook, G. Cunningham, E. Verwichte, and MAST Team, "Bi-directional Alfvén cyclotron instabilities in the mega-amp spherical tokamak," Phys. Plasmas **21**, 082501 (2014).
[41]H. Smith and E. D. Fredrickson, "Compressional Alfvén eigenmodes in rotating spherical tokamak plasmas," Plasma Phys. Controlled Fusion **59**, 035007 (2017).
[42]M. Ono, S. M. Kaye, Y.-K. M. Peng, G. Barnes, W. Blanchard, M. D. Carter, J. Chrzanowski, L. Dudek, R. Ewig, D. Gates, R. E. Hatcher, T. Jarboe, S. C. Jardin, D. Johnson, R. Kaita, M. Kalish, C. E. Kessel, H. W. Kugel, R. Maingi, R. Majeski, J. Manickam, B. McCormack, J. Menard, D. Mueller, B. A. Nelson, B. E. Nelson, C. Neumeyer, G. Oliaro, F. Paoletti, R. Parsells, E. Perry, N. Pomphrey, S. Ramakrishnan, R. Raman, G. Rewoldt, J. Robinson, A. L. Roquemore, P. Ryan, S. Sabbagh, D. Swain, E. J. Synakowski, M. Viola, M. Williams, J. R. Wilson, and NSTX Team, Nucl. Fusion **40**, 557 (2000).
[43]M. Ono, J. Chryzanowski, L. Dudek, S. Gerhardt, P. Heitzenroeder, R. Kaita, J. E. Menard, E. Perry, T. Stevenson, R. Strykowsky, P. Titus, A. von Halle, M. Williams, N. D. Atnafu, W. Blanchard, M. Cropper, A. Diallo, D. A. Gates, R. Ellis, K. Erickson, J. Hosea, R. Hatcher, S. Z. Jurczynski, S. Kaye, G. Labik, J. Lawson, B. LeBlanc, R. Maingi, C. Neumeyer, R. Raman, S. Raftopoulos, R. Ramakrishnan, A. L. Roquemore, S. A. Sabbagh, P. Sichta, H. Schneider, M. Smith, B. Stratton, V. Soukhanovskii, G. Taylor, K. Tresemer, A. Zolfaghari, and NSTX-U Team, Nucl. Fusion **55**, 073007 (2015).
[44]A. Pankin, D. McCune, R. Andre, G. Bateman, and A. Kritz, "The Tokamak Monte Carlo fast ion module NUBEAM in the national transport code collaboration library," Comput. Phys. Commun. **159**(3), 157–184 (2004).
[45]F. Poli, J. Sachdev, J. Breslau, M. Gorelenkova, and X. Yuan, "TRANSP," Computer Software, 27 June 2018.